Published in final edited form as:
NMR Biomed. 2012 January ; 25(1): 152–160. doi:10.1002/nbm.1727.

Regional Neurochemical Profiles in the Human Brain measured by ^{1}H MRS at 7 Tesla using Local B_1 Shimming

Uzay E. Emir[a], **Edward J. Auerbach**[a], **Pierre-Francois Van De Moortele**[a], **Małgorzata Marjańska**[a], **Kamil Uğurbil**[a], **Melissa Terpstra**[a], **Ivan Tkáč**[a], and **Gülin Öz**[a]

[a]Center for Magnetic Resonance Research, Department of Radiology, School of Medicine, University of Minnesota, Minneapolis, MN, USA

Abstract

Increased sensitivity and chemical shift dispersion at ultra-high magnetic fields (UHF) enable precise quantification of an extended range of brain metabolites from ^{1}H MR spectra. However, all previous neurochemical profiling studies using single-voxel MRS at 7 T were limited to data acquired from the occipital lobe with half-volume coils. Challenges of ^{1}H MRS of the human brain at 7 T include short T_2 and complex B_1 distribution that imposes limitations in maximum achievable B_1 strength. In this study, the feasibility of acquiring and quantifying short-echo (TE = 8 ms), single voxel ^{1}H MR spectra from multiple brain regions was demonstrated by utilizing a 16-channel transceiver array coil with 16 independent transmit channels allowing local transmit B_1 (B_1^+) shimming. Spectra were acquired from volumes-of-interest of 1 – 8 mL in brain regions that are of interest for various neurological disorders: frontal white matter, posterior cingulate, putamen, substantia nigra, pons and cerebellar vermis. Local B_1^+ shimming substantially increased transmit efficiency, especially in the peripheral and ventral brain regions. By optimizing a STEAM sequence for utilization with a 16-channel coil, artifact-free spectra were acquired with a small chemical shift displacement error (< 5% /ppm/direction) from all regions. The high SNR enabled the quantification of neurochemical profiles consisting of at least 9 metabolites including GABA, glutamate and glutathione in all brain regions. Significant differences in neurochemical profiles were observed between brain regions. For example, GABA levels were highest in the substantia nigra, total creatine highest in the cerebellar vermis and total choline highest in the pons, consistent with known biochemistry of these regions. These findings demonstrate that single voxel ^{1}H MRS at UHF can reliably detect region-specific neurochemical patterns in the human brain and has the potential to objectively detect alterations in neurochemical profiles associated with neurological diseases.

Keywords

MRS; B_1^+ shimming; short echo time; transceiver array coil; neurochemical profile; single voxel

Introduction

The advantages of ultra-high field (UHF) MR have been demonstrated in a variety of MR acquisition modalities (1). MRS can particularly benefit from substantial gains in signal-to-noise ratio (SNR) and spectral resolution at UHF, enabling the quantification of numerous metabolites from small volumes-of-interest (VOIs). For example, concentrations of up to 18 neurochemicals can be quantified from selected regions in the human brain at 7 T (2–4).

Correspondence to: Uzay Emir, Center for MR Research, 2021 6th St. S.E., Minneapolis, MN 55455, Tel: +1 612 626-2001, Fax: +1 612 626-2004, emirx001@umn.edu.

SNR is approximately two-fold and resolution 14% higher at 7 T relative to 4 T in the occipital cortex (2). As a result, metabolites are quantified with higher precision (lower Cramér-Rao Lower Bounds, CRLB) at 7 T than at 4 T, which is particularly critical for weakly represented neurochemicals (2). Despite this potential, short-echo ^{1}H MRS studies that reported neurochemical profiles of the human brain at 7 T were primarily focused on the occipital lobe (2–8) due to multiple challenges faced when using a standard volume head coil at UHF. First, the power to generate B_1 increases approximately linearly with magnetic field (9). As a result, the maximum magnitude of B_1^+ achievable with conventional volume head coils and available RF power are insufficient to generate conventional 90° or 180° RF pulses with bandwidths large enough to minimize chemical shift displacement errors in spectroscopy. This problem is exacerbated in large regions of the brain due to the destructive interferences that result in submaximal B_1^+ when volume coils circumscribing the whole head are used (10). Second, T_2 relaxation times of metabolites in the human brain are relatively short at this field (11,12) and the SNR advantages quickly disappear with increasing echo times. Therefore, short echo times are critical for quantifying neurochemical profiles and are particularly important for reliable quantification of metabolites with coupled spin systems, such as glutamine (Gln), glutamate (Glu) and glutathione (GSH).

New excitation and saturation pulses can be designed to partially overcome problems resulting from limitations in available B_1^+ magnitude. For example, MR spectroscopic imaging (MRSI) data were recently obtained using the FIDLOVS technique (13), based on 2D pre-localization by outer volume suppression (OVS) and slice-selective excitation with a newly designed broadband frequency-modulated RF pulse. Alternatively, the RF power required to achieve a given magnitude of B_1^+ in a local area can be reduced by utilizing an array of transmit coil elements and optimizing the phase and/or magnitude of RF delivered to each transmit element (B_1^+ shimming) (10,12,14,15). Recently, a similar approach has been employed to acquire MRSI data from brain slices at 7 T, demonstrating the feasibility of detecting *myo*-inositol (*myo*-Ins), Glu and Gln, in addition to N-acetylaspartate (NAA), creatine and choline (16,17). In these MRSI studies (13, 16, 17) relative metabolite concentrations were reported because acquisition of water reference data needed for absolute quantification would double the scan time. Another challenge with obtaining MRSI data for metabolite quantification is that efforts for improving the homogeneity of B_1^+ over a large volume generally result in decreased RF efficiency (18). On the other hand, in the single voxel spectroscopy approach, high RF efficiency to maximize B_1^+ over small VOIs can be readily achieved using local B_1^+ shimming, as was demonstrated in the human head at 9.4 T (12).

Another advantage of the single voxel approach is the ease with which the static magnetic field homogeneity can be adjusted. B_0 shimming is a key factor for successful MRS at 7 T, because it determines the achieved spectral resolution, which consequently affects the reliability of metabolite quantification. It has been demonstrated that a strong second-order shim system is sufficient to compensate B_0 inhomogeneities in reasonably small volumes (2,7). On the other hand, to achieve acceptable linewidths over the slice, the MRSI studies mentioned above (13,16,17) utilized third order B_0 shimming, a feature which is absent from most 7 T scanners, including our equipment. Therefore, in the absence of third or even higher order shims to attain sufficient B_0 homogeneity over large volumes in the brain, single voxel spectroscopy provides an alternative to MRSI for acquisition of very high quality spectra.

Finally, single voxel MRS might be preferable over the MRSI approach for clinical applications where the affected brain region is known and where motion artifacts are common (19–21). The phase and frequency instabilities induced by patient motion can be eliminated from single voxel MRS data by post-processing, provided that single scan spectra

are clean, and uncorrectable scans can be removed from the final FID summation (22). In addition, the single voxel approach allows one to abort the acquisition at any time and use the limited data set for metabolite quantification.

In this study, we tested the feasibility of acquiring and quantifying short-echo (TE = 8 ms), single voxel ^{1}H MR spectra from multiple brain regions utilizing the STEAM sequence (7,22), a 16-channel transceiver array coil (23) and local B_1^+ shimming at 7 T. Our goals were **1)** to determine if artifact free spectra of similar quality to those reported in the occipital lobe (2,7) could be obtained from brain regions that are of interest for various neurological disorders, namely the frontal white matter (demyelinating white matter diseases), posterior cingulate (Alzheimer's disease), putamen (Huntington's and Parkinson's diseases), substantia nigra (Parkinson's disease), pons (spinocerebellar ataxias, motor neuron diseases) and cerebellar vermis (spinocerebellar ataxias), and **2)** to quantify neurochemical profiles from these VOIs and to compare them to prior biochemical literature regarding neurochemical patterns in these regions.

Methods

Subjects

Fourteen healthy volunteers (8 females, 6 males, age (mean ± SD) = 32 ± 10) participated in this study after giving informed consent using procedures approved by the Institutional Review Board: Human Subjects Committee of the University of Minnesota.

MR Protocol

All measurements were performed on a 90-cm bore 7 T magnet (Magnex Scientific, Abingdon, UK) equipped with a head or body gradient coil (a maximum gradient amplitude of 40 mT/m and a slew rate of 170 mT/m/ms) and interfaced to a Siemens Syngo console (Siemens, Erlangen, Germany) with sixteen independent RF receivers. The body gradient coil included second-order shim coils with maximum shim strengths of $Z^2 = 6.2$ mT/m^2 and ZX, ZY, XY and X^2-$Y^2 = 2.5$ mT/m^2 at a current of 20 A, while all second order shim coils in the head gradient system had a strength of 6.2 mT/m^2 at a current of 20 A. A 16-channel transceiver array coil (23) was driven by sixteen 1 kW RF amplifiers (CPC, Brentwood, NY) which allowed independent control of phases and/or magnitudes of each transmit element of the array for B_1^+ shimming (24). 1 kW RF amplifiers were calibrated to deliver 900 W peak power, however only half of the transmitted power was actually available at the coil ports due to losses in cables and connectors. An in house built 16-channel monitoring system was used to continuously monitor the forward and reflected RF power on each channel which was averaged over two moving windows of 10 seconds and 10 minutes (12). If the power input into any coil element exceeded the predefined FDA threshold (3 / 16 Watts/kg/channel, conservatively assuming power deposition in only the head weighing ~ 4 kg), the scan was aborted. Besides the continuous RF power monitoring used during in vivo experiments, numeric electromagnetic simulations were also used to verify that global and local specific absorption rates (SAR) corresponding to our B_1^+ shimming approach were in compliance with U.S. Food and Drug Administration (FDA) guidelines. The 16-channel transceiver array coil loaded with a human head was modeled in the finite difference time domain (XFDTD, Remcom Inc, PA, USA). B_1^+ shimming solutions were performed within this model for VOIs defined in each of the anatomical target used in experiments, using the same B_1^+ phase shimming algorithm. For each corresponding B_1^+ shim solution the input power was scaled to match the experimentally measured B_1^+ value. Using the exact shape, amplitude and duration of each RF pulse used in the sequence for in vivo experiments, with same TR, SAR was then calculated over the head model. For each B_1^+ solution, global (over the whole head) and local (averaged over 1g of tissue) SAR values were always found

smaller than 3 Watts/kg and 8 Watts/kg, respectively, within FDA guidelines (data not shown) (25).

Before the MRS acquisition from each VOI, local B_1^+ shimming was performed over a region of interest (ROI) that encompassed the VOI. Low flip angle gradient echo (GRE) images were acquired for B_1^+ shimming when pulsing the RF power through one coil at a time, while the receive signal was sampled on all 16 channels (field of view (FOV) = 168 × 256 mm^2, repetition time (TR) = 60 ms, echo time (TE) = 3.6 ms, nominal flip angle (FA) = 15°, slice thickness 4 mm). The relative transmit B_1^+ phases were calculated using the B_1^+ phase formalism introduced by Van de Moortele et al (10). Local B_1^+ phase shimming was performed by averaging the phase of each channel over a ROI and then subtracting the normalized phase from the respective channel to minimize the destructive phase cancellation and maximize the fraction of available B_1^+. Note that the fraction of available B_1^+, which was defined as the ratio between the magnitude of the sum of the complex B_1^+ of each transmit channel and the sum of their magnitudes (14), can vary between 0 (when interferences are completely destructive) and 1 (when interferences are completely constructive). The predicted relative transmit efficiency (RTE) achievable with the local B_1^+ phase shimming technique relative to an initial transmit phase (set in 22.5 degree steps between adjacent elements) was calculated, based on the relative B_1^+ maps, from the postshim to preshim ratio of fraction of available B_1^+ averaged over the ROI (14). Note that only the phase, but not the magnitude, of each transmit channel was modulated relative to the others with our B_1^+ shimming algorithm.

Sagittal and transverse multislice images were acquired with a turbo spin echo sequence (FOV = 180 × 180 mm^2, TR = 3 s, TE = 93 ms, FA = 150 °, slice thickness 3 mm, 48 slices, one average) for selection of the VOI. First- and second-order shims were adjusted using FASTMAP (fast, automatic shimming technique by mapping along projections) with echo-planar imaging (EPI) readout (26). Spectra were measured by a short-echo STEAM sequence (TR = 5 s, TE = 8 ms, mixing time (TM) = 32 ms). The STEAM sequence combined with 3-D OVS and VAPOR (variable-power RF pulses with optimized relaxation delays) water suppression previously developed using a half-volume coil (22) was utilized with the following modifications: The asymmetric RF pulses used for STEAM slice selection were replaced by symmetric sinc RF pulses with broader bandwidth (1.5 ms, 5.9 kHz bandwidth) requiring a peak power B_1 of 34 μT ($\gamma B_1/2\pi$ = 1.46 kHz). In the previous work, a higher RF power was used for the OVS slab in y-dimension further away from the coil plane than the slab near the coil to account for the decrease in B_1^+ field with distance from the half-volume coil, whereas the same power magnitudes were used for the OVS pulses (hyperbolic secant, 5.0 ms, 8.4 kHz bandwidth) in each dimension here. The VAPOR water suppression parameters were unchanged from before (22) while crusher gradients were further optimized to provide artifact free spectra from all VOI. After the local B_1^+ phase shimming procedure for each VOI, the RF power magnitude for the 90° STEAM pulses was calibrated by monitoring the signal intensity while increasing the RF power and choosing the RF power setting that produced the maximum signal. The power magnitudes of OVS and VAPOR RF pulses were automatically set relative to the 90° STEAM pulses. Excellent water suppression in all brain regions, using the RF power setting derived from the STEAM RF power calibration, confirmed that a 90° flip angle of STEAM pulses, requiring a B_1^+ field of 34 μT was always reached. Spectra were acquired from 7 VOIs: occipital cortex (20 × 20 × 20 mm^3, number of transients (NT) = 128), posterior cingulate (20 × 20 × 20 mm^3, NT = 128), frontal white matter (20 × 20 × 20 mm^3, NT = 128), putamen (13 × 13 × 15 mm^3, NT = 256), substantia nigra (6 × 13 × 13 mm^3, NT = 512), pons (15 × 15 × 15 mm^3, NT = 256) and cerebellar vermis (10 × 25 × 25 mm^3, NT = 128), each from 5 healthy volunteers. The unsuppressed water signal acquired from the same VOI was used to remove residual eddy current effects and to reconstruct the phased array spectra (27). This included

weighting the spectra based on the sensitivity of each receive element at the VOI and correcting for the different constant phase shift terms of the complex spectra prior to the summation. Single scan spectra summed from 16 channels were corrected for frequency and phase variations induced by subject motion and then summed. When insufficient SNR did not permit correction of single acquisitions (in the pons, putamen and substantia nigra) data were averaged over 4 (pons and putamen) or 32 (substantia nigra) transients, corrected for frequency shifts and summed.

Metabolite quantification

Metabolites were quantified using LCModel (28,29). The model spectra of alanine (Ala), aspartate (Asp), ascorbate/vitamin C (Asc), glycerophosphocholine (GPC), phosphocholine (PC), creatine (Cr), phosphocreatine (PCr), γ-amino-butyric acid (GABA), glucose (Glc), Gln, Glu, GSH, *myo*-Ins, lactate (Lac), NAA, N-acetylaspartylglutamate (NAAG), phosphoethanolamine (PE), *scyllo*-inositol (*scyllo*-Ins) and taurine (Tau) were generated based on previously reported chemical shifts and coupling constants (30,31). Macromolecule spectra were acquired from the occipital cortex of 5 volunteers using an inversion recovery sequence (TR = 2 s, inversion time = 0.680 s) (32). Metabolite concentrations were obtained relative to an unsuppressed water spectrum acquired from the same VOI assuming a water content of 72% for frontal white matter and pons, 78% for putamen, 76% for substantia nigra and 82% for occipital cortex, posterior cingulate and cerebellar vermis, which primarily contain gray matter (33–35). Concentrations were not corrected for T_1 and T_2 effects and cerebrospinal fluid contribution to the VOI. Metabolites quantified with CRLB (estimated error of the metabolite quantification) > 50% were classified as not detected. Only metabolites quantified with CRLB ≤ 50% in at least three of the five spectra from a brain region were included in the final neurochemical profile. If the correlation between two metabolites was consistently high (correlation coefficient < −0.5) in a given region, their sum was reported, e.g. total creatine (Cr+PCr), total choline (GPC+PC) and Glc+Tau.

Statistics

One-way analysis of variance (ANOVA) with Tukey post hoc test was used to compare the concentrations at each of the seven locations for each metabolite.

Results

B_1^+ optimization

ROIs larger than and concentric with the selected VOIs were chosen to optimize the phases of the B_1^+ fields transmitted from each of the 16 channels. Two typical ROIs defined for local B_1^+ shimming are shown on transverse anatomical images in Figure 1A (occipital cortex) and D (substantia nigra). The phases of channels 1 through 16 were set to 0 to 360° in increments of 22.5° before local B_1^+ shimming. Low flip angle GRE images were utilized to generate relative B_1^+ maps both before and after implementation of local B_1^+ shim phases to evaluate the predicted RTE within the ROI. For instance, in the occipital cortex, a region in the periphery of the brain, 34% of the available B_1^+ was realized before B_1^+ shimming (Fig. 1B). After B_1^+ shimming, 89% of the available B_1^+ was realized within the same ROI (Fig. 1C), corresponding to a predicted RTE of 2.64. On the other hand, in the substantia nigra, a more central region in the brain, the fractions of available B_1^+ before and after B_1^+ shimming were 73% and 84%, respectively, and the predicted RTE was 1.16. The averages of predicted RTE values are shown in Table 1 for all brain regions. These values were even higher when calculating the average B_1^+ after local B_1^+ shimming only within the VOI used for spectroscopy, since the maximum B_1^+ efficiency was obtained in the center of the ROI

(Fig. 1). That a B_1^+ of at least 34 μT was available for all brain regions was confirmed directly by calibration of the RF pulses in STEAM.

Pulse sequence optimization

The modifications in the STEAM sequence relative to the one previously developed using a half-volume coil (22) provided optimum performance with the 16-channel transceiver array coil. First, the broader bandwidth symmetric sinc RF pulses used for slice selection resulted in slightly reduced chemical shift displacement error (< 5% /ppm/direction). Second, equal OVS power magnitudes in each dimension provided optimum suppression of signal from outside of the VOI because the B_1^+ field of the 16-channel coil after local B_1^+ shimming was almost symmetric around the VOI in every dimension. Third, the VAPOR water suppression parameters previously optimized for minimum sensitivity to T_1 and $B1^+$ variation (22) provided optimum water suppression with the 16-channel coil as well. Finally, crusher gradients used for STEAM, OVS and VAPOR adjusted to suppress unwanted stimulated echoes resulted in artifact-free spectra from all brain regions studied (Fig. 2).

Spectral quality

Figure 2 shows representative spectra obtained from different brain regions at 7 T. In all brain regions, the residual water signal was smaller than the major metabolite peaks. In addition, the double localization accomplished by STEAM and OVS eliminated signals from outside the VOI, such as lipid signals from the subcutaneous tissue, which resulted in artifact-free spectra with a flat baseline. This excellent quality was consistently achieved in all brain regions (Fig. 2). Localized B_0 shimming using FASTMAP resulted in water linewidths (full width at half maximum (FWHM)) ranging from 11 Hz (in posterior cingulate) to 18 Hz (in substantia nigra) (Table 2).

Neurochemical profiles

The mean concentrations of metabolites that met our criteria for reliable quantification in at least six of the seven brain regions are shown in Figure 3A. Both the sum and individual values are reported for NAA and NAAG because these metabolites could be reliably distinguished (correlation coefficient between concentrations less negative than −0.5, Fig. 4) in all regions with CRLB < 10% except substantia nigra and putamen (correlation coefficient ~ −0.65, CRLB < 30%). Eight other metabolites (GABA, Glu, GSH, *myo*-Ins, *scyllo*-Ins, Cr+PCr, GPC+PC and Glc+Tau) were quantified with average CRLB ranging between 1–35% in all brain regions (Fig. 3B). Asc, Gln and Lac were quantified reliably in all brain regions (CRLB < 30%) except substantia nigra.

The comparison of metabolite concentrations revealed neurochemical profiles characteristic of different brain regions (Fig. 3A). For instance, the GABA level in the substantia nigra (2.5 ± 0.15 μmol/g) was 2–3 fold higher ($p < 0.001$) than the other brain regions (0.5 – 1.8 μmol/g). The cerebellar vermis had the highest total creatine (12.8 ± 0.8 μmol/g, $p < 0.001$) and Glc+Tau level (5.1 ± 0.1, μmol/g, $p < 0.001$). A high (GPC+PC)/(Cr+PCr) ratio was apparent from the pons spectrum (Fig. 2), which resulted primarily from higher total choline (2.9 ± 0.3 μmol/g) than other regions. Total NAA (NAA + NAAG) was fairly uniformly distributed between regions (11.6 – 13.6 μmol/g). The lowest Glu level was in the substantia nigra (5.9 ± 0.5 μmol/g) and the highest Glu levels were observed in the posterior cingulate and putamen (10.8 ± 0.5 and 10.7 ± 0.3 μmol/g, respectively). The highest *myo*-Ins levels were quantified in the pons and the cerebellar vermis (8.4 ± 0.7 and 9.1 ± 1.1 μmol/g, respectively). The GSH level varied from 0.50 ± 0.1 μmol/g (occipital cortex) to 1.2 ± 0.2 μmol/g (cerebellar vermis) and the *scyllo*-Ins varied from 0.2 ± 0.1 μmol/g (frontal white matter) to 0.5 ± 0.1 μmol/g (substantia nigra).

Discussion

This study demonstrated that high quality single-voxel short-echo STEAM spectra can be obtained from clinically relevant brain regions at 7 T using a transceiver array coil and local B_1^+ shimming. Importantly, our 7 T scanner is operated with a clinical console, demonstrating the feasibility of implementing the technology on clinical platforms. The spectral quality previously reported in the occipital cortex at 7 T using a half-volume RF coil (2,7) was reproduced with a 16-channel transceiver array coil (Fig. 2). In addition, spectra of high quality were acquired from other brain regions affected in various neurological disorders. Neurochemical profiles quantified from these spectra were consistent with biochemical literature (see below). To our knowledge, these extended profiles of region specific neurochemical concentrations are reported at 7 T for the first time.

Previously, single voxel, short-echo ^{1}H MRS studies at 7 T utilized half-volume coils and therefore reported neurochemical profiles of only the occipital cortex in humans (2–7,22). Flexibility in selecting VOIs, especially deeper in the brain requires the use of volume head coils for both transmission and detection. This, however, creates challenges because the B_1 distribution in the human head for a volume coil is extremely non-uniform (9,10,36,37). In the center of the brain, transmit and receive B_1 associated with individual current carrying elements of the volume coil add approximately in phase resulting in highest possible B_1 (10,36); however, B_1 fields generated by the individual current carrying elements tend to cancel each other in the periphery and ventral regions of the brain due to destructive interferences. In this study, we utilized a transceiver array coil driven by a multichannel transmit system, which allowed local B_1^+ shimming to minimize the B_1^+ losses. Optimizing the transmit phases in the individual coil channels enabled to maximize the available B_1^+ magnitude in the selected VOIs (Fig. 1). The predicted RTE values ranged from 1.2 in the substantia nigra to 3.3 in the cerebellar vermis (Table 2). These results are in agreement with the fact that at UHF, constructive interferences yield increased magnitude of B_1^+ field in the center of the brain, whereas destructive interferences cause a reduction in magnitude of B_1^+ field in the periphery of the brain (10). Thus, in this study, VOIs selected in the periphery of the brain and especially in the cerebellum benefited more substantially from B_1^+ shimming than VOIs in the center of the brain.

The hardware available in this study (a 16-channel transceiver array coil driven by sixteen 1 kW RF amplifiers) and improved RTE by local B_1^+ shimming provided a transmit field of at least 34 μT in all studied brain regions, which was confirmed directly by calibration of the RF pulses in STEAM. The available peak B_1^+ field combined with high bandwidth RF pulses resulted in a reasonably low chemical shift displacement error (< 5% /ppm/direction). In general, if sufficiently high B_1^+ is not achievable, extending the duration of RF pulses in the MRS localization sequence is necessary. However, chemical shift displacement errors at UHF quickly become unacceptably large with increasing RF pulse length and decreasing bandwidths when conventional, amplitude modulated RF pulses are utilized. Another possibility for reducing the chemical shift displacement error when B_1^+ is low is to use broadband adiabatic RF pulses for slice selection (38,39). However, slice selective adiabatic excitation pulses are currently not available; therefore the localization must be achieved with multiple inversion pulses at the expense of much longer TE as in the LASER technique (38) or by forgoing single shot acquisition as in the ISIS method (40,41).

For this study, the STEAM sequence was chosen despite the loss of half of the available signal, primarily to minimize relaxation effects at an ultra-short echo time, but also to have a low chemical shift displacement artifact and to compare spectral quality and metabolite quantification to previously published work in the occipital cortex at 7 T (2–4,7,22). Transverse relaxation at long TE results in substantial signal loss at higher fields since the

Hahn T_2 of metabolites decreases with increasing field strength due to an increased dynamic dephasing contribution (11,12). For instance, the T_2 of NAA decreases from 240 ms at 4 T to 160 ms at 7 T (11). Thus, even a modest increase of TE from 8 to 30 ms would lead to a 12% lower NAA signal at 7 T. In addition, J-evolution was minimized at the ultra-short TE, which facilitated the quantification of metabolites with coupled spin systems.

To achieve high spectral resolution at 7 T, efficient B_0 shimming is very important. In this study, the strength of the second-order shim system combined with efficient B_0 shimming (FASTMAP) resulted in highly reproducible linewidths in the selected VOIs. This was shown by less than 15% standard deviation of the water signal linewidth in all brain regions (Table 2). Considering an increase in linewidth at 7 T by a factor of 1.5 relative to 4 T (2), the linewidths obtained in the substantia nigra were in agreement with published results for substantia nigra at 4 T (21). Similarly, the previously reported linewidths for the occipital cortex at 7 T (2) were reproduced in the current study. Linewidths obtained in the substantia nigra, putamen and frontal white matter were substantially higher than those in the other VOIs due to the effects of high iron content in the substantia nigra and putamen (42) and global magnetic field inhomogeneity in frontal white matter due to the close proximity of the nasal air cavities.

The achieved spectral quality (high spectral resolution, SNR, excellent localization performance, efficient water suppression, and a distortionless baseline) allowed reliable quantification of 17 metabolites in occipital cortex (VOI = 8 mL) using LCModel analysis. Concentrations of metabolites quantified in this study were in good agreement with recently reported values acquired from the same brain location using a very similar approach except for the RF coil (2). The average difference between concentrations obtained in the current study and the prior report was only 0.25 μmol/g.

Nine metabolites were reliably estimated using LCModel analysis in all studied brain regions. In addition, nine metabolites were quantified with average CRLB less than 20% in 5 of the 7 brain regions studied (Fig. 3B), indicating that these were the most robustly quantified neurochemicals. In general, changes in neurochemical levels greater than twice the CRLB can be detected in individual spectra with 95% confidence (43). Hence, disease related alterations in those metabolites quantified with CRLB above 20% can only be detected if the effect sizes are quite large (more than twice the CRLB).

Comparison of metabolite concentrations between different brain regions revealed significant regional variations (Fig. 3). The findings were in excellent agreement with prior neurochemical and MRS studies of anatomical locations most similar to those presented here. For example, the high cerebellar total creatine level was in agreement with previous reports (20,44–46). In addition, the highest Glc+Tau concentration obtained in cerebellar vermis was consistent with high cerebellar Tau (47) and Glc (48) levels reported relative to other brain regions. Confirming previous MRS studies (44,49), the highest total choline levels were observed in the pons and the lowest total choline levels were measured in the occipital cortex. The concentration of total NAA had a fairly homogenous distribution, consistent with previous MRS studies (44,49). The GABA level was significantly higher in the substantia nigra than other regions, also in agreement with both MRS (21) and neurochemistry literature (47). High *myo*-Ins concentrations in the pons and vermis were also consistent with prior MRS literature (46).

In conclusion, the combination of a multichannel transceiver array coil and local B_1^+ shimming enabled us to acquire excellent single voxel, short-echo STEAM spectra from multiple brain regions at 7 T. The high spectral quality facilitated the quantification of neurochemical profiles consisting of at least nine metabolites including GABA, Glu and

GSH. These findings demonstrate that single voxel ^{1}H MRS at 7 T can reliably detect region-specific neurochemical patterns in the human brain and has the potential of becoming an objective tool to monitor neurochemical profile alterations associated with several neurological diseases.

Acknowledgments

We thank the staff of the Center for MR Research for maintaining and supporting the MR system, in particular Dr. Gregor Adriany for assistance with the 16-channel coil and the 7 T scanner. We would like to thank Can Akgun for his invaluable assistance with the SAR simulations. This work was supported by the Dana Foundation (G.Ö.) and National Institute on Aging research grant R21 AG029582 (M.T.). The Center for MR Research is supported by the National Center for Research Resources (NCRR) biotechnology research resource grant P41 RR008079, the Neuroscience Center Core Blueprint Award P30 NS057091 and Keck Foundation. Coil support was provided by the National Institute of Biomedical Imaging and Bioengineering grant R01 EB006835 (J. Thomas Vaughan).

Abbreviations Used

Ala	alanine
Asc	ascorbate
Asp	aspartate
Cr	creatine
CRLB	Cramér-Rao lower bounds
FA	flip angle
FOV	field of view
FWHM	full width at half maximum
GABA	γ-aminobutyric acid
Glc	glucose
Gln	glutamine
GPC	glycerophosphocholine
GRE	gradient echo
GSH	glutathione
Glu	glutamate
Lac	lactate
MRSI	magnetic resonance spectroscopic imaging
***myo*-Ins**	*myo*-inositol
NAA	N-acetylaspartate
NAAG	N-acetylaspartylglutamate
NT	number of transients
OVS	outer volume suppression
PC	phosphocholine
PCr	phosphocreatine
PE	phosphoethanolamine
ROI	region of interest

RTE	relative transmit efficiency
SAR	specific absorption rate
***scyllo*-Ins**	*scyllo*-inositol
SNR	signal-to-noise ratio
Tau	taurine; TE, echo time
TE	echo time
TM	mixing time
TR	repetition time
UHF	ultra high field
VAPOR	variable-power RF pulses with optimized relaxation delays
VOI	volume of interest

References

1. Uğurbil K, Adriany G, Andersen P, Chen W, Garwood M, Gruetter R, Henry PG, Kim SG, Lieu H, Tkáč I, Vaughan T, Van De Moortele PF, Yacoub E, Zhu XH. Ultrahigh field magnetic resonance imaging and spectroscopy. Magn Reson Imaging. 2003; 21(10):1263–1281. [PubMed: 14725934]
2. Tkáč I, Öz G, Adriany G, Uğurbil K, Gruetter R. In vivo ^{1}H NMR spectroscopy of the human brain at high magnetic fields: metabolite quantification at 4T vs. 7T. Magn Reson Med. 2009; 62(4):868–879. [PubMed: 19591201]
3. Mangia S, Tkáč I, Gruetter R, Van De Moortele PF, Giove F, Maraviglia B, Uğurbil K. Sensitivity of single-voxel ^{1}H-MRS in investigating the metabolism of the activated human visual cortex at 7 T. Magn Reson Imaging. 2006; 24(4):343–348. [PubMed: 16677939]
4. Terpstra M, Uğurbil K, Tkáč I. Noninvasive quantification of human brain ascorbate concentration using ^{1}H NMR spectroscopy at 7 T. NMR Biomed. 2010; 23(3):227–232. [PubMed: 19655342]
5. Mekle R, Mlynárik V, Gambarota G, Hergt M, Krueger G, Gruetter R. MR spectroscopy of the human brain with enhanced signal intensity at ultrashort echo times on a clinical platform at 3T and 7T. Magn Reson Med. 2009; 61(6):1279–1285. [PubMed: 19319893]
6. Gambarota G, Mekle R, Xin L, Hergt M, van der Zwaag W, Krueger G, Gruetter R. In vivo measurement of glycine with short echo-time ^{1}H MRS in human brain at 7 T. MAGMA. 2009; 22(1):1–4. [PubMed: 18949497]
7. Tkáč I, Andersen P, Adriany G, Merkle H, Uğurbil K, Gruetter R. In vivo ^{1}H NMR spectroscopy of the human brain at 7 T. Magn Reson Med. 2001; 46(3):451–456. [PubMed: 11550235]
8. Scheenen TW, Heerschap A, Klomp DW. Towards ^{1}H-MRSI of the human brain at 7T with slice-selective adiabatic refocusing pulses. MAGMA. 2008; 21(1–2):95–101. [PubMed: 18210177]
9. Vaughan JT, Garwood M, Collins CM, Liu W, DelaBarre L, Adriany G, Andersen P, Merkle H, Goebel R, Smith MB, Uğurbil K. 7T vs. 4T: RF power, homogeneity, and signal-to-noise comparison in head images. Magn Reson Med. 2001; 46(1):24–30. [PubMed: 11443707]
10. Van de Moortele PF, Akgün C, Adriany G, Moeller S, Ritter J, Collins CM, Smith MB, Vaughan JT, Uğurbil K. B_1 destructive interferences and spatial phase patterns at 7 T with a head transceiver array coil. Magn Reson Med. 2005; 54(6):1503–1518. [PubMed: 16270333]
11. Michaeli S, Garwood M, Zhu XH, DelaBarre L, Andersen P, Adriany G, Merkle H, Uğurbil K, Chen W. Proton T_2 relaxation study of water, N-acetylaspartate, and creatine in human brain using Hahn and Carr-Purcell spin echoes at 4T and 7T. Magn Reson Med. 2002; 47(4):629–633. [PubMed: 11948722]
12. Deelchand DK, Van de Moortele PF, Adriany G, Iltis I, Andersen P, Strupp JP, Vaughan JT, Ugurbil K, Henry PG. In vivo 1H NMR spectroscopy of the human brain at 9.4 T: initial results. J Magn Reson. 2010; 206(1):74–80. [PubMed: 20598925]

13. Henning A, Fuchs A, Murdoch JB, Boesiger P. Slice-selective FID acquisition, localized by outer volume suppression (FIDLOVS) for ^{1}H-MRSI of the human brain at 7 T with minimal signal loss. NMR Biomed. 2009; 22(7):683–696. [PubMed: 19259944]
14. Metzger GJ, Snyder C, Akgün C, Vaughan T, Uğurbil K, Van de Moortele PF. Local B_1^+ shimming for prostate imaging with transceiver arrays at 7T based on subject-dependent transmit phase measurements. Magn Reson Med. 2008; 59(2):396–409. [PubMed: 18228604]
15. Van de Moortele, PF.; Snyder, C.; DelaBarre, L.; Akgün, C.; Wu, X.; Vaughan, JT.; Uğurbil, K. Biomedical Magnetic Resonance Imaging and Spectroscopy at Very High Fields. Würzburg: 2006. Fast mapping of relative B_1 phase in the human head at 9.4 Tesla with a 14 channel transceive coil array.
16. Hetherington HP, Avdievich NI, Kuznetsov AM, Pan JW. RF shimming for spectroscopic localization in the human brain at 7 T. Magn Reson Med. 2010; 63(1):9–19. [PubMed: 19918903]
17. Avdievich NI, Pan JW, Baehring JM, Spencer DD, Hetherington HP. Short echo spectroscopic imaging of the human brain at 7T using transceiver arrays. Magn Reson Med. 2009; 62(1):17–25. [PubMed: 19365851]
18. Mao W, Smith MB, Collins CM. Exploring the limits of RF shimming for high-field MRI of the human head. Magn Reson Med. 2006; 56(4):918–922. [PubMed: 16958070]
19. Öz G, Tkáč I, Charnas LR, Choi IY, Bjoraker KJ, Shapiro EG, Gruetter R. Assessment of adrenoleukodystrophy lesions by high field MRS in non-sedated pediatric patients. Neurology. 2005; 64(3):434–441. [PubMed: 15699371]
20. Öz G, Hutter D, Tkáč I, Clark HB, Gross MD, Jiang H, Eberly LE, Bushara KO, Gomez CM. Neurochemical alterations in spinocerebellar ataxia type 1 and their correlations with clinical status. Mov Disord. 2010
21. Öz G, Terpstra M, Tkáč I, Aia P, Lowary J, Tuite PJ, Gruetter R. Proton MRS of the unilateral substantia nigra in the human brain at 4 tesla: detection of high GABA concentrations. Magn Reson Med. 2006; 55(2):296–301. [PubMed: 16408282]
22. Tkáč I, Gruetter R. Methodology of 1H NMR Spectroscopy of the Human Brain at Very High Magnetic Fields. Appl Magn Reson. 2005; 29(1):139–157. [PubMed: 20179773]
23. Adriany G, Van de Moortele PF, Ritter J, Moeller S, Auerbach EJ, Akgün C, Snyder CJ, Vaughan T, Uğurbil K. A geometrically adjustable 16-channel transmit/receive transmission line array for improved RF efficiency and parallel imaging performance at 7 Tesla. Magn Reson Med. 2008; 59(3):590–597. [PubMed: 18219635]
24. Vaughan JT, Snyder CJ, DelaBarre LJ, Bolan PJ, Tian J, Bolinger L, Adriany G, Andersen P, Strupp J, Uğurbil K. Whole-body imaging at 7T: preliminary results. Magn Reson Med. 2009; 61(1):244–248. [PubMed: 19097214]
25. U.S. Department of Health and Human Services Food and Drug Administration; 2010 December 17. Guidance for Industry and FDA Staff: Criteria for Significant Risk Investigations of Magnetic Resonance Diagnostic Devices. http://wwwfdagov/MedicalDevices/DeviceRegulationandGuidance/GuidanceDocuments/ucm072686htm
26. Gruetter R, Tkáč I. Field mapping without reference scan using asymmetric echo-planar techniques. Magn Reson Med. 2000; 43(2):319–323. [PubMed: 10680699]
27. Natt O, Bezkorovaynyy V, Michaelis T, Frahm J. Use of phased array coils for a determination of absolute metabolite concentrations. Magn Reson Med. 2005; 53(1):3–8. [PubMed: 15690495]
28. Provencher SW. Estimation of metabolite concentrations from localized in vivo proton NMR spectra. Magn Reson Med. 1993; 30(6):672–679. [PubMed: 8139448]
29. Provencher SW. Automatic quantitation of localized in vivo ^{1}H spectra with LCModel. NMR Biomed. 2001; 14(4):260–264. [PubMed: 11410943]
30. Govindaraju V, Young K, Maudsley AA. Proton NMR chemical shifts and coupling constants for brain metabolites. NMR Biomed. 2000; 13(3):129–153. [PubMed: 10861994]
31. Tkáč, I. Refinement of simulated basis set for LCModel analysis. Proceedings 16th Scientific Meeting, International Society for Magnetic Resonance in Medicine; Toronto. 2008. p. 1624
32. Behar KL, Rothman DL, Spencer DD, Petroff OA. Analysis of macromolecule resonances in 1H NMR spectra of human brain. Magn Reson Med. 1994; 32(3):294–302. [PubMed: 7984061]

33. Randall LO. Chemical topography of the brain. J Biol Chem. 1938; 124:481–488.
34. Gelman N, Ewing JR, Gorell JM, Spickler EM, Solomon EG. Interregional variation of longitudinal relaxation rates in human brain at 3.0 T: relation to estimated iron and water contents. Magn Reson Med. 2001; 45(1):71–79. [PubMed: 11146488]
35. Siegel, GJ., editor. Basic neurochemistry: molecular, cellular and medical aspects. Philadelphia: Lippincott-Raven Publishers; 1999.
36. Collins CM, Liu W, Schreiber W, Yang QX, Smith MB. Central brightening due to constructive interference with, without, and despite dielectric resonance. J Magn Reson Imaging. 2005; 21(2): 192–196. [PubMed: 15666397]
37. Yang QX, Wang J, Zhang X, Collins CM, Smith MB, Liu H, Zhu XH, Vaughan JT, Uğurbil K, Chen W. Analysis of wave behavior in lossy dielectric samples at high field. Magn Reson Med. 2002; 47(5):982–989. [PubMed: 11979578]
38. Garwood M, DelaBarre L. The return of the frequency sweep: designing adiabatic pulses for contemporary NMR. J Magn Reson. 2001; 153(2):155–177. [PubMed: 11740891]
39. Tannus A, Garwood M. Adiabatic pulses. NMR Biomed. 1997; 10(8):423–434. [PubMed: 9542739]
40. Ordidge RJ, Connelly A, Lohman JAB. Image-selected in Vivo spectroscopy (ISIS). A new technique for spatially selective nmr spectroscopy. Journal of Magnetic Resonance. 1986; 66(2): 283–294.
41. Mlynárik V, Gambarota G, Frenkel H, Gruetter R. Localized short-echo-time proton MR spectroscopy with full signal-intensity acquisition. Magn Reson Med. 2006; 56(5):965–970. [PubMed: 16991116]
42. Riederer P, Sofic E, Rausch WD, Schmidt B, Reynolds GP, Jellinger K, Youdim MB. Transition metals, ferritin, glutathione, and ascorbic acid in parkinsonian brains. J Neurochem. 1989; 52(2): 515–520. [PubMed: 2911028]
43. Provencher SW. LCModel & LCMgui User's Manual. 2001
44. Baker EH, Basso G, Barker PB, Smith MA, Bonekamp D, Horska A. Regional apparent metabolite concentrations in young adult brain measured by ^{1}H MR spectroscopy at 3 Tesla. J Magn Reson Imaging. 2008; 27(3):489–499. [PubMed: 18307197]
45. Pouwels PJ, Frahm J. Regional metabolite concentrations in human brain as determined by quantitative localized proton MRS. Magn Reson Med. 1998; 39(1):53–60. [PubMed: 9438437]
46. Viau M, Marchand L, Bard C, Boulanger Y. ^{1}H magnetic resonance spectroscopy of autosomal ataxias. Brain Res. 2005; 1049(2):191–202. [PubMed: 15963476]
47. Perry, TL. Cerebral amino acid pools. In: Lajtha, A., editor. Handbook of Neurochemistry. 2nd ed. Volume 1. New York: Plenum Press; 1982. p. 151-180.
48. Swanson RA, Sagar SM, Sharp FR. Regional brain glycogen stores and metabolism during complete global ischaemia. Neurol Res. 1989; 11(1):24–28. [PubMed: 2565546]
49. Jacobs MA, Horska A, van Zijl PC, Barker PB. Quantitative proton MR spectroscopic imaging of normal human cerebellum and brain stem. Magn Reson Med. 2001; 46(4):699–705. [PubMed: 11590646]

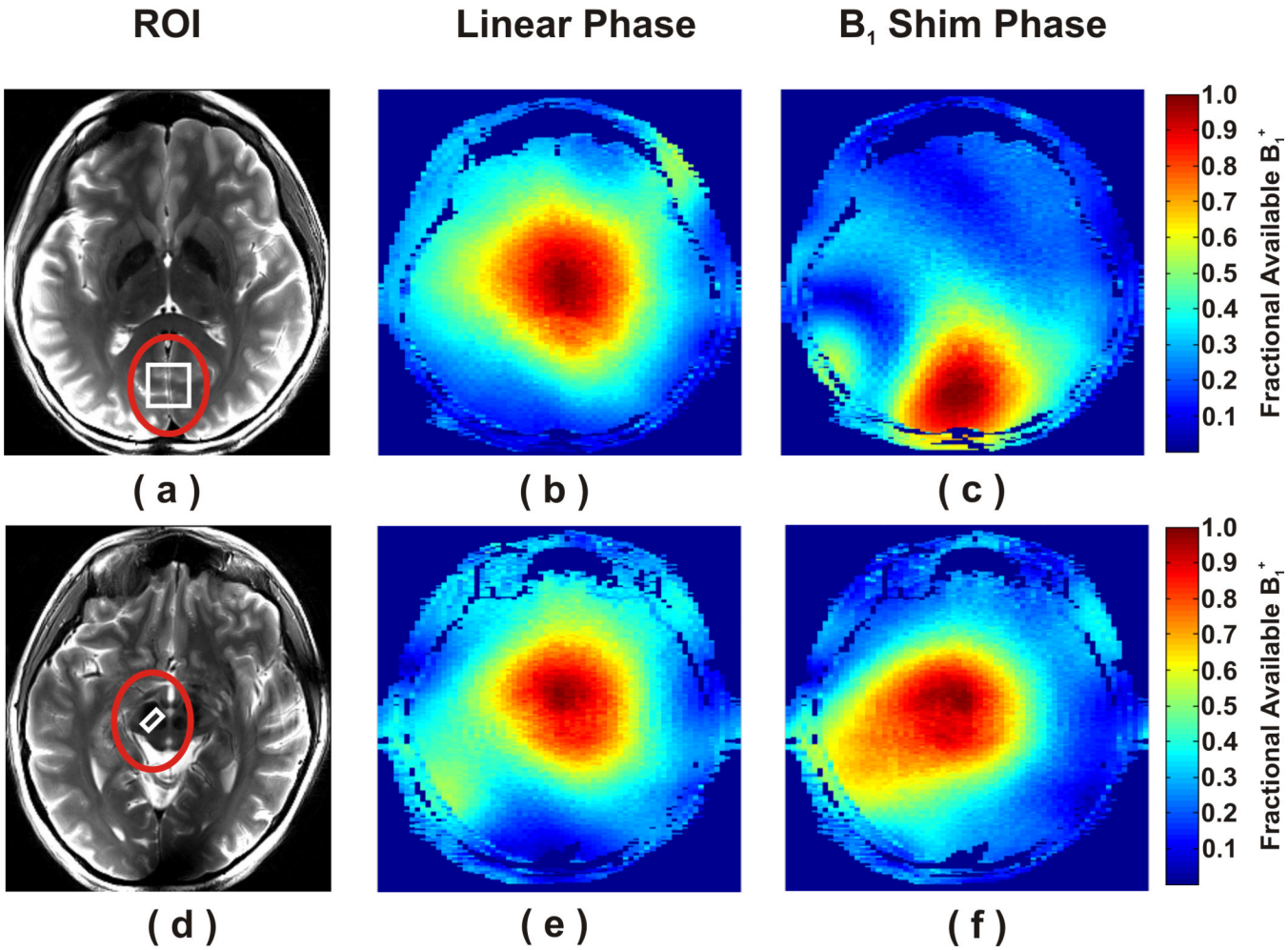

Figure 1.
Local B_1^+ shimming at the periphery (a) and center of one subject's brain (d). The ROIs (red circles) were used to shim B_1^+ for the VOIs (white squares); (a) occipital cortex and (d) substantia nigra. Maps of the fraction of available B_1^+ before (b, e) and after (c, f) B_1^+ shimming are shown for the occipital cortex (b,c) and substantia nigra (e, f).

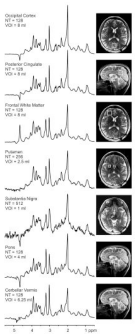

Figure 2.

^{1}H MR spectra obtained with STEAM (TR = 5 s, TE = 8 ms, TM = 32 ms) from seven VOIs. The spectra were scaled based on neurochemical concentrations obtained by LCModel. Processing: Reconstruction of single scan FIDs from phased array data, frequency and phase correction of FID arrays, FID summation, correction for residual eddy current effects, Gaussian multiplication (σ = 0.1 s), Fourier Transform (FT), zero-order phase correction. Positions of the VOIs are shown on T_2 – weighted images. (NT = number of transients)

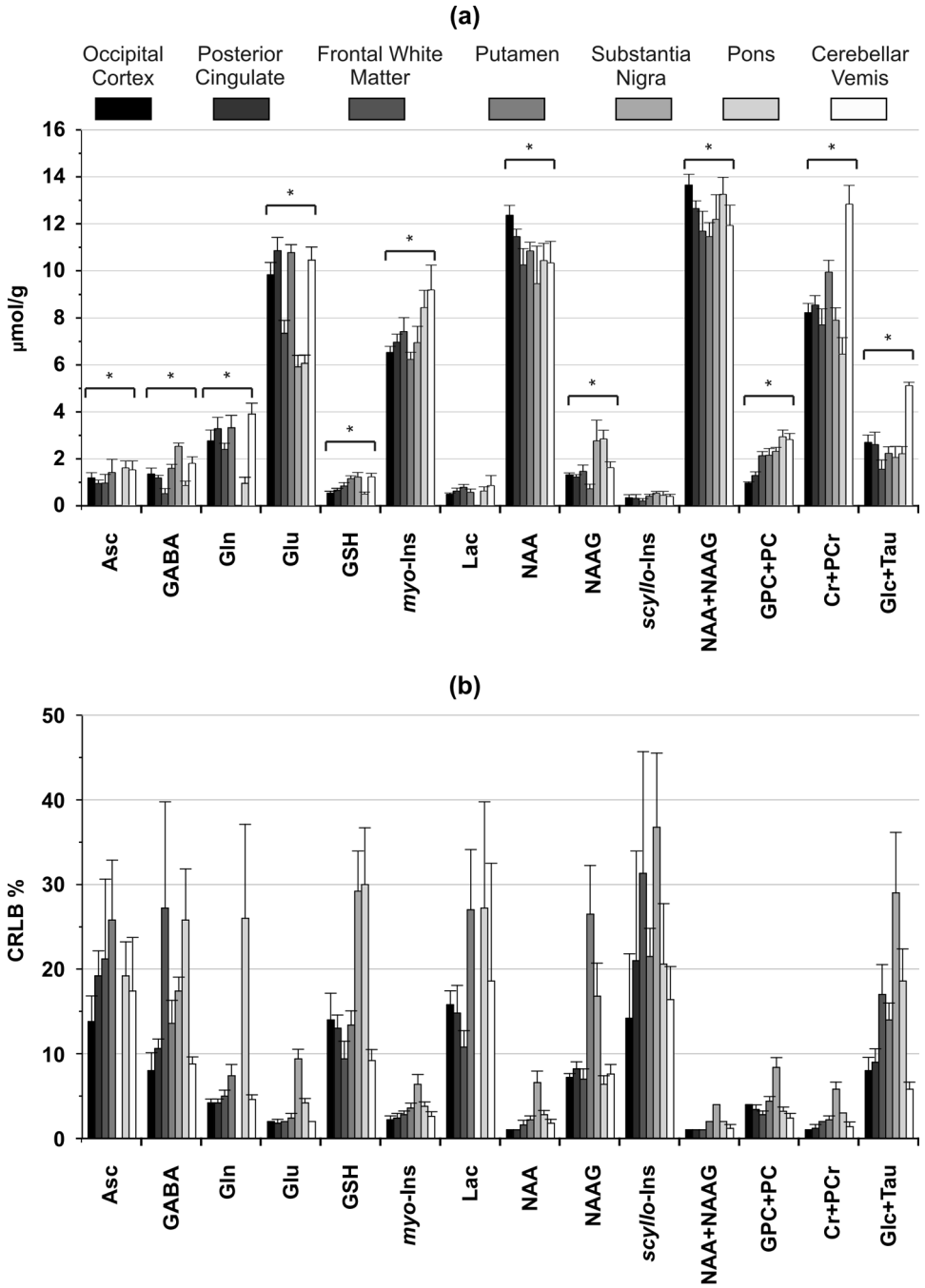

Figure 3.

Neurochemical profiles and corresponding CRLBs from different brain regions determined by LCModel fitting of short-echo STEAM spectra acquired at 7 T. (a) Only metabolites that were quantified reliably (with CRLB ≤ 50% in at least three of the five spectra from a brain region) in at least six of the seven brain regions are shown. Metabolites that were significantly different between regions are marked with: * $p < 0.005$ (ANOVA). (b) CRLBs expressed in relative units (%). Error bars: inter-subject SD (N=5 for all brain regions).

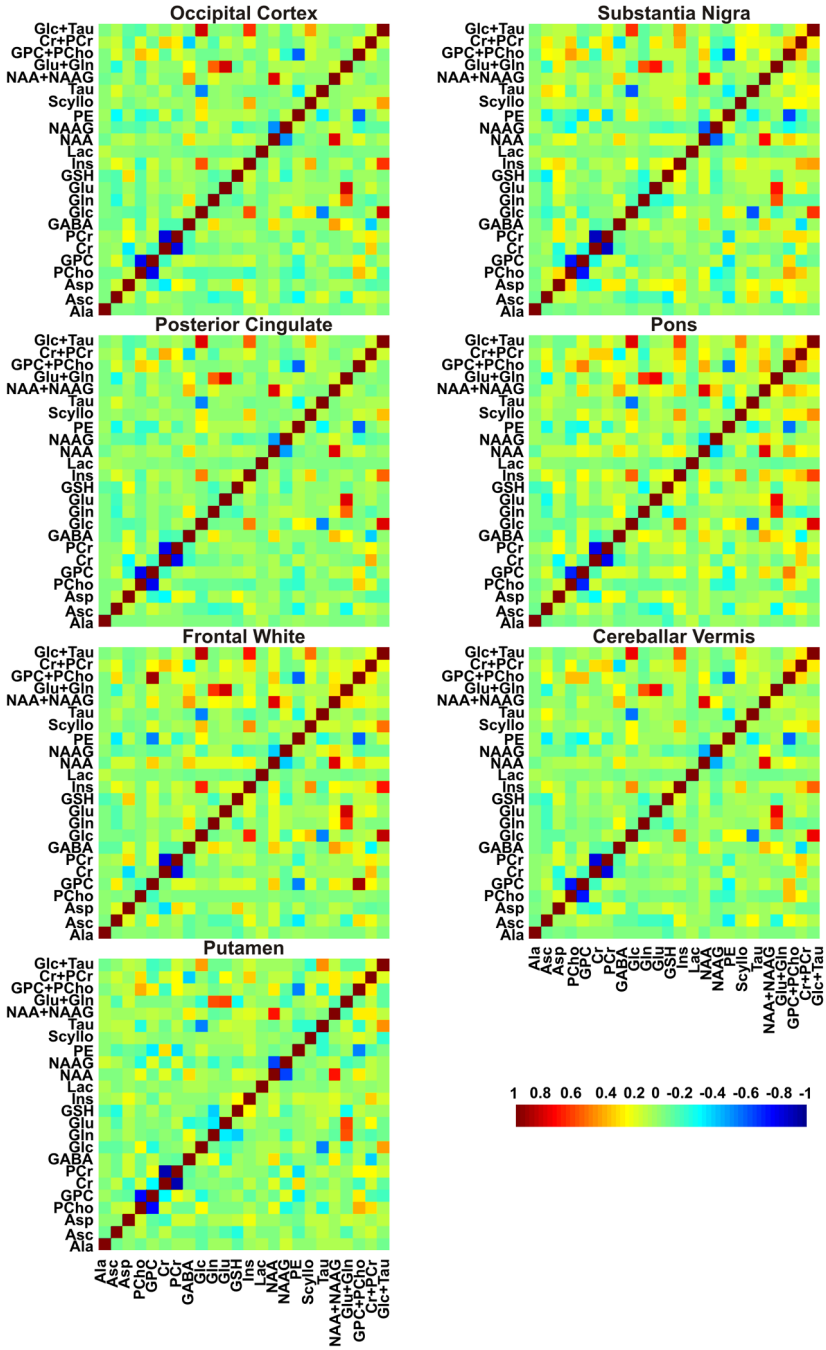

Figure 4.

Mean correlation coefficients matrices between the metabolite concentrations in different brain regions determined by LCModel fitting of short-echo STEAM spectra acquired at 7 T. Non-zero off-diagonal elements of the correlation coefficients matrices indicate the level of covariance between the fitting results for the corresponding two metabolites.

Table 1

Relative transmit efficiencies (RTE), i.e. ratios (mean ± SD) of the B_1^+ maps after to before B_1^+ shimming, averaged over the different regions of interest.

Region of Interest	RTE (After / Before B_1^+ shimming)
Occipital cortex	2.5 ± 0.2
Posterior cingulate	1.4 ± 0.4
Frontal white matter	1.9 ± 0.2
Putamen	1.6 ± 0.2
Substantia nigra	1.2 ± 0.1
Pons	1.3 ± 0.1
Cerebellar vermis	3.3 ± 0.3

Table 2

Water signal linewidths (mean ± SD) achieved in the different volumes of interest.

Volume of Interest	FWHM (Hz)
Occipital cortex	12.7 ± 0.3
Posterior cingulate	11.3 ± 0.7
Frontal white matter	15.7 ± 0.8
Putamen	15.9 ± 1.2
Substantia nigra	18.0 ± 1.0
Pons	14.3 ± 1.9
Cerebellar vermis	14.5 ± 0.6